LA-UR-19-26791 (Accepted Manuscript)

Automated co-adding and energy calibration of large array microcalorimeter data with zero sample knowledge

Yoho, Michael Duncan
Garner, Scott Edward
Koehler, Katrina Elizabeth
Vo, Duc Ta
Croce, Mark Philip

To be published in: Nuclear Instruments and Methods in Physics Research Section A: Accelerators, Spectrometers, Detectors and Associated Equipment

DOI to publisher's version: 10.1016/j.nima.2020.164056

Permalink to record: http://permalink.lanl.gov/object/view?what=info:lanl-repo/lareport/LA-UR-19-26791

Automated Co-Adding and Energy Calibration of Large Array Microcalorimeter Data with Zero Sample Knowledge

M. D. Yoho[a], K. E. Koehler[a,*], S. E. Garner[a], D. T. Vo[a], M. P. Croce[a]

[a] *Los Alamos National Laboratory, Los Alamos, NM 87545, USA*

Abstract

State-of-the-art microcalorimeter spectrometers now contain large detector arrays with hundreds of individual pixels. Each individual pixel outputs a unique and non-linear response with respect to deposited energy. This work describes a pattern-recognition algorithm to combine these responses into a single energy-calibrated histogram, referred to as co-adding pixels. Photo-peaks from different pixels are matched together based upon how well the match aligns the centroids and heights of neighboring peaks. This usually results in around 100 co-adding calibration points from 30 to 300 keV for a several day acquisition of plutonium items with masses between 0.5 and 10 grams. An additional algorithm energy-calibrates this co-added spectrum using the fluoresced K x-ray emissions from a tantalum absorber and inherent x-ray escape peaks from the tin absorbers. Both algorithms operate without knowledge of the source and are fully automated. This work presents results from the acquisitions of high and low burnup plutonium, 10% enriched uranium, a ^{153}Gd calibration source, and a ^{57}Co+^{166m}Ho calibration source. In all measurements, resolution defined as the full-width at half-maximum (FWHM) of photo-peaks is preserved between the individual pixel and co-added spectra at around 65 eV for incident photon energies between 60 and 208 keV. The energy calibration algorithm is approximate

*Corresponding author
Tel.: +1 (505) 695 4100
Email: kkoehler@lanl.gov

and yields a calibration curve off by an average of around 200 eV for incident photon energies between 60 and 208 keV.

Keywords: Microcalorimeter, transition edge sensor, co-adding, array, calibration

1. Introduction

Advancements in microwave frequency-division multiplexing, a low-noise method of reading out multiple pixels on a single feed line, are well described in [1–4]. This has allowed the construction of large superconducting transition-edge sensor (TES) arrays such as the 256-pixel microcalorimeter described in [5], which have counting efficiencies approaching those of high-purity germanium (HPGe) detectors for photon energies between 30 and 208 keV. The uniqueness, non-linearity, and transient nature of individual pixel responses is further described in [6, 7]. Post-acquisition, waveform data must be processed to produce a final histogrammed energy spectrum. This task necessitates the co-adding of a large number of individual spectra, each with a different non-linear energy response. This co-adding must also be very precise in order to preserve the excellent sub-100 eV resolution of the individual pixels. One possible data processing methodology is described in [8]. Waveforms are initially processed to produce list-mode data, typically using an optimal Wiener filter [9]. The list-mode data from each pixel are then histogrammed. Observed photo-peaks are then matched to known photon emission energies emitted from the known source. For plutonium, typically around six energies are used for this calibration. The individual energy-calibrated spectra are then co-added to produce a single final spectrum.

This approach has several disadvantages that make it difficult to apply in many real-world applications. First, it requires an already well-characterized sample. This assumption is perfectly acceptable in applications such as stockpile stewardship where, for example, measurements of plutonium sources of similar isotopic composition are carried out on a daily basis. However, this assump-

tion may not apply in applications such as nuclear forensics where a detection system must be capable of analyzing a range of materials from thorium [10] to uranium [11] to post-detonation debris [12] where there exists no a-priori source knowledge. Second, co-adding pixel responses together based upon a small set of known energies may decrease the resolution of potentially useful forensics and safeguards signatures at other energies. For example, if pixelated data from a fission sample such as trinitite is only co-added based upon the 59, 129, and 208 keV photon signatures of plutonium, then potential fission-product signatures from ^{133}Ba at 81 keV, ^{152}Eu at 122 keV, and ^{154}Eu at 123 keV may be of too poor resolution for either qualitative or quantitative analysis.

This work addresses these two disadvantages by reversing the analysis flow-of-work described in [8]. Pixelated spectra are first co-added using a pattern-recognition algorithm that requires no sample knowledge. The algorithm matches all photo-peaks from differing pixels, provided that the peaks have a high confidence of resulting from the same photon signature. A match achieves a high confidence if it makes the centroids and heights of neighboring peaks line up. For plutonium, typically 80 to 110 photo-peaks are chosen, resulting in a very well co-added spectrum with co-added energy resolutions from 30 to 208 keV similar to the average pixel resolution.

Once a single co-added spectrum exists, then any energy-calibration technique can be used to scale the list-mode data. This work describes a novel approach using fluoresced K x-rays (56.3, 57.3, 64.9 and 65.2 keV) from a tantalum absorber placed between the source and detector as well as tin escape photo-peaks throughout the spectrum. This methodology is consistent with the zero-source knowledge approach of the co-adding algorithm.

A primary photo-peak and the associated tin escape peak will differ in energy by 25.3 keV. The measurement of the photo-peak and escape-peak centroids gives a secant line representing the average change in energy over a change in Wiener filter value. The slope of the secant therefore approximates the derivative of the energy calibration curve. The integral of this derivative will therefore approximate the energy calibration curve.

Energy calibration accuracy (off by at most 0.5 keV for plutonium, uranium, and commercial calibration sources considered in this work) suffices for many traditional safeguards applications. For example, the plutonium isotopic analysis code FRAM developed at Los Alamos requires energy calibration accuracy of around 0.6 keV at 100 keV and 0.9 keV at 208 keV for HPGe spectra [13]. However, the accuracy is not as good as achieved by matching peak energies to those of known nuclides.

Since there is only a single spectrum to calibrate and energy calibration does not affect resolution, it is also quite easy for an experienced scientist to calibrate by hand. Micro-View, a graphical user interface written in python, allows a user to double-click on peaks to determine their centroids and match these centroids to known energies in an isotopic library. The list-mode data is then transformed using a cubic spline function with the matched pairs as knots. The result is a perfectly linear and energy-calibrated spectrum. The drawback of this methodology is the requirement of a resident spectroscopy expert.

2. Experimental

A set of plutonium and uranium reference materials and radiation calibration sources were measured in order to test co-adding and automated energy-calibration performance. Three different plutonium sources, a ^{57}Co+^{166m}Ho source, a ^{153}Gd source, and a 10% enriched uranium source were measured with the SLEDGEHAMMER array (Spectrometer to Leverage Extensive Development of Gamma-ray TESs for Huge Arrays using Microwave Multiplexed Enabled Readout) [14] within the SOFIA (Spectrometer Optimized for Facility Integrated Applications) cryostat [15]. The transition edge sensors (TESs) in this array are Mo-Cu bilayers with super conducting transitions around 110 mK. All the sources were measured at an operating temperature of 80 mK with a transition-edge sensor (TES) bias of 1.2 V. The sources were placed as close to the cryostat window as possible to maximize the count rate. Count rates per pixel were generally below around five counts per second to minimize pileup

issues. For all acquisitions, a 0.1 mm tantalum sheet was placed between the source and detector to generate x-rays for energy calibration. For the plutonium sources, a 0.5 to 1.5 mm cadmium sheet was placed between the source and the detector to reduce the high count rate from the 59.54 keV ^{241}Am gamma-ray. Acquisition times varied between a few hours to several days. Table 1 describes the six measured items and contains information about the measurement process.

Table 1: Description of sources and measuring conditions. The count time (T) is given in hours. N is the total counts and N_p is the number of pixels passing cuts.

Item	Description	Amount	T	N	N_p
PIDIE-6	PUO_2 (25% ^{240}Pu)	0.4 g	92	9.7×10^7	149
^{153}Gd	Commercial	1 μCi	2	4.9×10^5	134
PIDIE-1	PUO_2 (6% ^{240}Pu)	0.4 g	83	1.6×10^8	144
^{166m}Ho + ^{57}Co	Commercial	1 μCi	22	3.7×10^7	84
CBNM-61	PUO_2 (27% ^{240}Pu)	10.5 g	49	7.8×10^7	145
A1-324-1	UO_2 (10% en.)	1 kg	100	2.6×10^7	92

Post-acquisition, waveforms were processed via an optimal Wiener filter, pixels with poor performance were cut from the analysis, and list-mode data was drift-corrected in a manner similar to [8]. After drift-correction, the list-mode data was subject to the co-adding and energy calibration routines described in this work. Subsets of 8-hours of waveform data were also processed in a similar manner to test co-adding and energy calibration performance for typical counting times expected for a 24 hour nuclear forensics report or laboratory safeguards measurements.

Fitting parameters (Gaussian σ and left and right exponential parameters τ_L and τ_R from a two-tailed Bortels fit [16]) were determined for important and isolated photo-peaks in the spectra for each pixel as well as the co-added spectrum. These individual and co-added fitting parameters were compared to determine if resolution is preserved during the co-adding process. A left and

right-tailed Bortels function on top of a linear background shape was assumed for the photo-peaks [17]. Calibrated centroids of various important peaks for forensics and safeguards located throughout the summed spectra were also recorded and compared to tabulated values from the National Nuclear Data Center [18].

3. Co-adding algorithm

The co-adding algorithm relies on three assumptions concerning pixel response.

Similar heights. The co-adding algorithm assumes all the pixels have efficiencies within an order of magnitude of each-other. This assumption is necessary to use the height information of spectral features for co-adding. Sometimes, an individual pixel is very inefficient (no recorded events) at low or high energies. In these cases, the co-adding algorithm will only match together peaks in the middle energy range of the spectrum.

Gradual curvature. The co-adding algorithm further assumes the derivative of energy with respect to Wiener filter value (dE/dW) for any pixel changes slowly. For the MoCu TES and tin absorbers used in this work, it is assumed that dE/dW can change by no more than around 20% from 20 to 350 keV.

Similar resolution. Currently, the algorithm works well for pixels with peak widths within a factor of three of each other, such that kernel widths for peak detection and centroid detection can be the same for all pixels. If a pixel has very poor resolution, then the kernel width may be sub-optimal, and peak detection is less likely to work well.

3.1. Preliminaries

Initially, individual pixel responses may be quite different. For example, some pixels may have three times the gain as other pixels. That is, Wiener filter values corresponding to the 59 keV photon signature from ^{241}Am may be three times higher in magnitude for some pixels than for others. This may lead

to sub-optimal performance. For example, peak detection kernel widths may be sub-optimal and lead to many false-negative and false-positive identifications. To address this, the average Wiener filter value for each pixel as well as the global average is determined. Then, the list-mode data for each pixel is scaled by the ratio of the global average to the individual average. This ensures scaled Wiener filter values for all of the pixels corresponding to the same energy signature will all be within roughly 50% of each-other.

The list-mode data is then histogrammed so that roughly three histogram channels correspond to the average FWHM of gamma-ray signatures. This rather coarse binning is to ensure adequate performance for very low-statistics spectra. If a measurement system will only take long, high statistics measurements, then a finer binning structure may result in better co-added resolution.

Peaks are found above background by applying a second-order, second-derivative Savitsky-Golay filter [19–21] to the histogrammed data. The kernel width is four times the assumed average FWHM of the system. Peak centroids are then further refined by interpolating the zero-crossings of a second-order, first-derivative Savitsky-Golay filter with a kernel width twice the assumed average FWHM. Heights are taken as the second-derivative filter values at the peak centroid position. Taking actual peak heights works, but the second-derivative has already filtered out the slowly changing background underneath the photopeaks. At the conclusion of these preliminaries, each pixel has a list of peak centroids and second derivative filter values corresponding to heights.

3.2. Determination of template spectrum

The algorithm chooses a template pixel. All other pixel responses will be transformed to the template pixel response. It is a good idea to try to choose a pixel with desirable properties such as good resolution, efficiency, low amount of drift, and a good linear response with respect to energy. Left and right-tailed Bortels functions [17] on a linear background are fit to the largest peak in each spectrum in order to estimate resolution. Pixels are then given a resolution rank (r_{res}) ranging from 1 (best resolution) to 256 (worst resolution). In a

similar manner, pixels are given an efficiency score (r_{eff}) based upon the total number of photons detected. This should be sufficient to pick a decent template pixel. In this work to improve energy calibration performance, pixels are further given a third rank according to the magnitude of the drift correction (r_{drift}). Finally, pixels are given a linearity rank (r_{lin}) according to how correlated the average pulse heights are to the Wiener filter values. The average pulse height is a component of the E-Joule linear energy calibration metric described in [22]. This relationship to E-Joule suggests average pulse height is more linearly correlated to incident photon energy. Therefore, pixels whose Wiener filter values are highly correlated to average pulse height may be more correlated to energy. Each pixel is then given a total rank (r_{total}):

$$r_{\text{total}} = (r_{\text{res}})^2 + (r_{\text{eff}})^2 + (r_{\text{drift}})^2 + (r_{\text{lin}})^2 \tag{1}$$

The pixel with the numerically lowest rank is then chosen as the template spectrum. The addition in quadrature is to ensure a template pixel with no obvious weaknesses.

3.3. Candidate peaks

To improve algorithm speed, it is necessary to choose a small subset of the peaks in the template spectrum which may match to a small subset of the peaks in a subordinate spectrum. This is done by choosing the top five tallest peaks in the template spectrum and the top five tallest peaks in the subordinate spectrum. It is highly likely there will be at least one peak in the subordinate spectrum that matches a peak in the template spectrum.

3.4. Neighborhoods

A candidate peak in the subordinate spectrum will be matched to a candidate peak in the template spectrum. A match is good if it leads to good alignment of centroids and heights of surrounding peaks in the subordinate spectrum to surrounding peaks in the template spectrum within certain neighborhoods. In this work, each peak is assigned a neighborhood that encompasses the five closest

peaks. Fewer neighbors than three increases the chance of noise misidentified as a peak affecting a good match.

3.5. Iterations

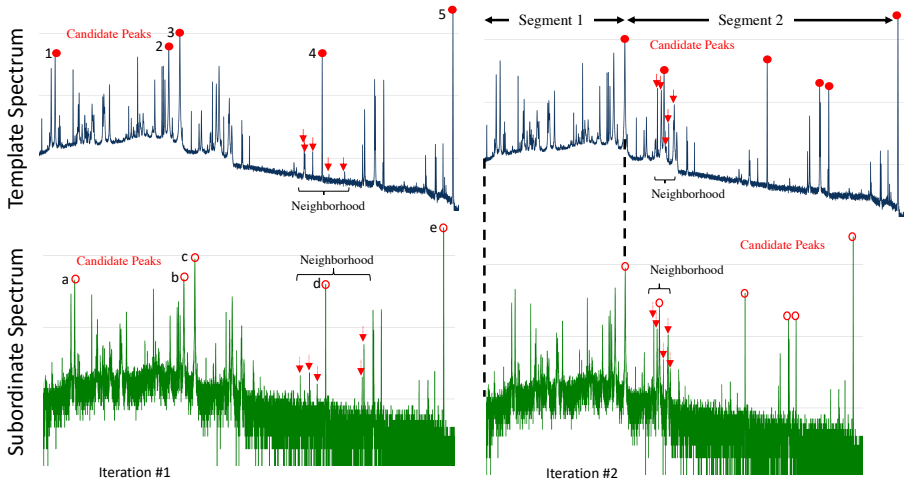

Figure 1: A schematic of the co-adding matching algorithm. The five tallest peaks in both the template spectrum (1,2,3,4,5) and the subordinate spectrum (a,b,c,d,e) are chosen as candidate peaks. Each candidate peak in the subordinate spectrum is tested against every candidate peak in the template spectrum (e.g. 1-a, 1-b, 1-c, 1-d, 1-e, 2-a, et.c) for a match. A match is the pair with the highest score based on scoring how well the neighborhoods (five closest peaks to the candidate peak) matched using fuzzy logic (see Section 3.6). Once a match has been determined, this forms a knot in the mapping function (g) along with the origin. With a knot fixed, the next iteration has two new segments and within each segment new candidate peaks are chosen and matched using the same approach.

As can be seen in Figure 1, after the candidate peaks in the subordinate spectrum are scored with the candidate peaks in the template spectrum, the top scoring pair is considered a match. The first good match will divide the subordinate spectrum into two halves below and above the chosen subordinate peak. The good match will also divide the template spectrum into two halves above and below the chosen template peak. A relative gain mapping g is then generated from the subordinate spectrum to the template spectrum. This work uses a cubic spline function with the matches as knots. The origin is always

considered a spline knot since it is reasonable that a Wiener filter value of zero will always map to an energy of zero keV no matter which pixel is considered. For the first initial match, g is a straight line. A relative efficiency curve ϵ is also generated between knot peak heights. In this work, ϵ is a linear interpolation function and for the first iteration it is a flat line.

The second iteration will choose five new subordinate spectrum peak candidates below the chosen knot and five new template spectrum peak candidates below the chosen knot. Another good match in this segment will add a new knot to the relative mapping functions g and ϵ. The algorithm repeats and continues adding more knots and further dividing the subordinate spectrum and template spectrum into more numerous and smaller search segments. In this manner, very high-confidence matches are chosen first, usually between very large and distinct peaks, and smaller peaks are chosen later. However, the smaller peaks will also likely be matched together since the mapping functions g and ϵ will be known to a high degree of precision and the search regions for matches will be very small. Eventually, there will only be segments left containing one or two peaks.

To become a good match, a candidate match must have a score (described in section 3.6) of at least 0.25 and further be 33% higher than any other candidate match containing the same peak from either the template or subordinate spectrum. This reduces the chances of a false positive match. Only the candidate match with the highest score may become a good match. If no candidate match is deemed a good match in a particular segment, then it will be considered again after the rest of the segments are searched for good matches. A second examination with more accurate mapping functions g and ϵ may generate a good match. The algorithm terminates when a full sweep through all segments yields no new matches. For plutonium, this typically occurs after around 100 peaks are matched.

3.6. Scoring

Each candidate match between a candidate peak P_s in the subordinate spectrum and a candidate peak P_t in the template spectrum is given a score $S(P_t, P_s)$. This score is based upon how well neighbor centroids and heights align if the centroids and heights of P_s and P_t are added to the current g and ϵ curves. Scoring is done using fuzzy logic [23]. Temporarily, g and ϵ are given an extra knot containing the candidate match and become g' and ϵ'. For a candidate match, each possible combination of i neighbors in the subordinate spectrum and j neighbors in the template spectrum is given a height sub-score $H(i,j)$ and a centroid sub-score $C(i,j)$ based upon these temporary g' and ϵ' curves.

The height sub-score, $H(i,j)$, is essentially the ratio of the heights of neighbors i and j divided by the ratio of the heights of candidate peaks P_t and P_s:

$$H(i,j) = \frac{\epsilon'(h_i)}{h_j} \cdot \frac{h_{P_t}}{\epsilon'(h_{P_s})}. \tag{2}$$

The addition of an efficiency curve improves scoring accuracy. If the neighboring peaks originate from the same photon signature and the candidate peaks originate from the same photon signature then $H(i,j) \approx 1$. Here, h_i, h_j, h_{P_s}, and h_{P_t} are the heights associated with i, j, P_j, and P_s. Note that if $H(i,j) > 1$ then it is inverted so the sub-score always ranges from 0 to 1.

The centroid sub-score, $C(i,j)$, uses a simple triangular fuzzy logic scoring system and is defined as:

$$C(i,j) = 1 - \frac{|g'(c_i) - c_j|}{3 \cdot FWHM}, \tag{3}$$

where the centroids of i and j are denoted by c_i and c_j, respectively. The lowest score achievable is $C(i,j) = 0$. This is achieved when the distance between the two centroids, scaled by g', is three times the system FWHM. If $C(i,j) < 0$, then it is set equal to 0, so the score is always between 0 and 1. Thus, centroids separated by more than three times the system FWHM are also given a centroid sub-score of 0. If the two centroids align perfectly, then $C(i,j) = 1$—a perfect centroid sub-score.

The individual sub-score, $I(P_t, P_s)$, is addressed in a similar manner to neighbor sub-scoring:

$$I(P_t, P_s) = \frac{\epsilon(h_{P_s})}{h_{P_t}} \left(1 - \frac{|g(c_{P_s}) - c_{P_t}|}{3 \cdot FWHM}\right), \tag{4}$$

where c_{P_s} and c_{P_t} denote the centroids of P_s and P_t, respectively. Sometimes there are peaks that do not have any close neighbors. This may happen for low statistics reactor-grade plutonium spectra where the 208 keV peak from ^{241}Pu and ^{241}Am is detected but the 203 keV peak from ^{239}Pu is below the noise level. Neighboring peaks will be very far away and contribute little valuable information. Therefore, it helps to introduce an individual sub-score based upon how well the centroids and heights of P_t and P_s align given g and ϵ. The overall score, $S(P_t, P_s)$, for a particular candidate match is defined as

$$S(P_t, P_s) = I(P_t, P_s) + \sum_{i=1}^{5} \sum_{j=1}^{5} H(i, j) C(i, j). \tag{5}$$

A special case occurs when a neighbor is also a peak from a known good match determined in a prior iteration. In this case, this known good match must itself be temporarily omitted from the working gain and efficiency curves.

3.7. Co-added Histogram

After determining all of the good matches, the list-mode data from the subordinate spectrum is transformed with the relative gain curve, g. The algorithm then determines the resolutions of the peaks in the subordinate spectra that map to the largest peak in the template spectrum. Spectra that have resolutions two standard deviations above the average pixel resolution are removed from subsequent analysis. The transformed list-mode data are then histogrammed and summed together to produce a single spectrum.

4. Energy calibration algorithm

The energy calibration algorithm uses fluoresced tantalum x-rays for lower energy calibration and uses tin x-ray escape peaks for higher energy calibration.

The tantalum Kα_2, Kα_1, Kβ_3, and Kβ_1 x-ray energies at 56.3, 57.5, 64.9, and 65.2 keV, respectively, are visible in a PIDIE-6 plutonium measurement as seen in Figure 2. Note the distinctive and easy to identify 4-peak pattern spanning the 59.5 keV ^{241}Am peak. All combinations of four identified photo-peaks in the co-added spectrum are checked to see how well their centroids match this 4-peak pattern and how well their heights match the x-ray relative emission intensities per 100 K-shell vacancies. A fuzzy logic scoring system similar to that described in Section 3.6 is used to determine which combination corresponds to the true tantalum x-rays. The energy calibration curve E is then taken as a polynomial fit through these four known energy–Wiener-filter-value pairs.

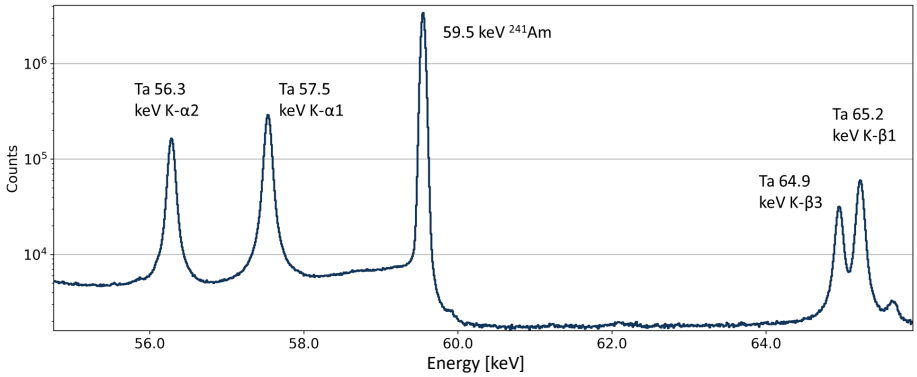

Figure 2: Ta x-rays spanning the ^{241}Am 59.5 keV peak in a PIDIE-6 plutonium spectrum.

Tin x-ray escape peaks comprise roughly 10% of the area of the full photo-electric absorption peaks between 60 and 208 keV for the 380 μm thick absorbers used in this work. The Kα_1 and Kα_2 x-ray escapes with energies of 25.0 and 25.3 keV, respectively, form a distinctive doublet. A doublet x-ray escape 25 keV below the 185.7 keV photo-peak from ^{235}U can be seen in Figure 3.

The energy calibration algorithm locates these K x-ray doublets associated with the primary photo-peaks with a fuzzy logic scoring described in section 3.6. The Kα_2 escape and primary photo-electric responses form a secant line which estimates the derivative of the energy calibration curve at the midpoint

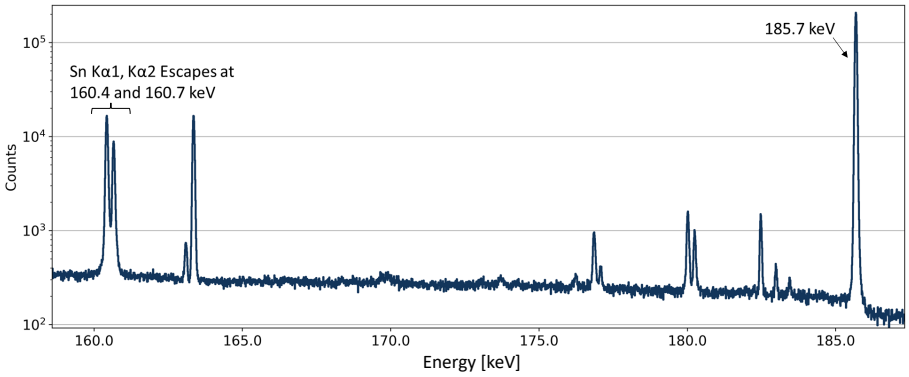

Figure 3: Sn Kα_1 and Kα_2 x-ray escape peaks 25.0 and 25.3 keV below the ^{235}U 185.7 keV full photo-electric peak.

of the secant. Equation 6 describes this derivative approximation:

$$\frac{dE}{dw}(w = (w_p + w_e)/2) \approx \frac{25.3 \text{ keV}}{w_p - w_e}, \tag{6}$$

where w_p and w_e represent the Wiener filter centroids associated with the primary photo-peak and escape peak, respectively.

The algorithm typically locates around four tin escape peak responses for the plutonium, uranium, and commercial calibration sources examined in this work below 220 keV. The continuous function $\frac{dE}{dw}$ is then constructed by generating a linear interpolation function using the secant estimates as knots. The energy calibration curve E above the last Wiener-filter value w_0 corresponding to the highest tantalum x-ray at 65.2 keV is then determined by integrating $\frac{dE}{dw}$:

$$E(w) = w_0 + \int_{w_0}^{w} dw' \frac{dE}{dw'}(w') \tag{7}$$

Since a secant is only an approximation of a derivative, the energy calibration curve, $E(w)$, is less precise than fitting a curve through a set of known points.

5. Results

Resolution and calibrated centroid energies for prominent and important photo-peaks are provided for the eight-hour data-set (Table 2) and the full

acquisition data set (Table 3). For both the short and long analyses, the average FWHM from 60 to 208 keV is around 65 eV in the co-added spectrum. Absolute calibrated centroid errors are typically around 200 eV for longer acquisitions. It is necessary to have a sufficient number of detected photons to detect the tin x-rays. For the eight-hour analysis of PIDIE-1, the counting statistics of the 208 keV ^{241}Pu/^{241}Am photo-peak and corresponding tin escape peaks are too low to construct a secant line and estimate the energy calibration curve derivative. This method will only generate a decent energy calibration curve where there are prominent photo-peaks; thus, the energy calibration curve is not as accurate above around 130 keV.

Table 4 (8-hour data set) and Table 5 (full acquisition data set) demonstrate that resolution is essentially preserved during the co-adding process. The average FWHM of individual pixel photo-peaks are similar to the co-added FWHM and differ by no more than a few eV. Tables 4–5 also demonstrate that σ is reduced during the co-adding process whereas tailing increases in magnitude. Usually, there are a large number of good pixels with resolutions around 45–65 eV and a few bad pixels with much poorer resolutions 100 eV or higher. When these are summed together, there will be a narrow Gaussian component which is due to the summing of the good pixels. The few poor resolution pixels manifest as tailing in the summed spectral feature. This suggests it is good to fit a two-tailed Bortels function to co-added spectra to take into account these tails instead of a symmetric Gaussian.

A close-up of the co-added 10% enriched A1-324-1 uranium spectrum around 95 keV is depicted in Figure 4. Note the clear separation of the ^{238}U signatures at 92.4 and 92.8 keV and the ^{235}U signature at 93.35 keV which are typically used to determine enrichment in non-destructive assay. The uranium spectrum from 50 to 205 keV is depicted in Figure 5. Co-added and energy-calibrated spectra for the six long acquisitions and the five eight-hour analyses are included in the supplementary information.

The single-button user interface for automated co-adding and energy calibration named Micro Matcher Zero can be seen in Figure 6. We also show

a screenshot of a second analysis software package, Micro-View, which allows manual energy calibration, isotope identification, and basic quantitative analysis capability.

Table 2: Resolution and energy calibrated centroids for 8-hour data set. The difference between the centroid energy from literature (E_{lit}) and the calibrated centroid (E_{cal}) is ΔE. The FWHM refers to the FWHM of the peak in the co-added spectrum.

Item	Isotope	E_{lit} [keV]	E_{cal} [keV]	FWHM [eV]	ΔE [eV]
PIDIE-6	^{241}Am	59.54	59.55	60	10
	^{240}Pu	104.23	104.07	61	160
	^{239}Pu	129.3	129.22	64	80
	^{241}Pu	208	207.62	64	380
PIDIE-1	^{241}Am	59.54	59.57	59	30
	^{240}Pu	104.23	104.24	63	10
	^{239}Pu	129.3	128.89	61	410
	^{241}Pu	208	204.46	60	3540
^{166m}Ho/^{57}Co	^{166m}Ho	80.57	80.78	66	210
	^{57}Co	122.06	122.4	66	340
	^{166m}Ho	184.41	184.91	65	500
CBNM61	^{241}Am	59.54	59.57	67	30
	^{240}Pu	104.23	104.08	64	150
	^{239}Pu	129.3	129.29	74	10
	^{241}Pu	208	208.29	70	290
A1-324-1	^{235}U	143.76	143.31	67	448
	^{235}U	185.71	185.37	64	340
			Averages:	64.7	408.1
			Worst:	74	3540

6. Conclusions

This work describes a fully automated large detector array co-adding algorithm that works with microcalorimetr data. Resolution is preserved during the co-adding process. Co-added resolutions measured as photo-peak FWHM range from 60 to 75 eV from 60 to 208 keV for measurements of plutonium, uranium, and commercial calibration sources. This algorithm does not rely on any

Table 3: Resolution and energy calibrated centroids for full acquisition data set. The difference between the centroid energy from literature (E_{lit}) and the calibrated centroid (E_{cal}) is ΔE. The FWHM refers to the FWHM of the peak in the co-added spectrum.

Item	Isotope	E_{lit} [keV]	E_{cal} [keV]	FWHM [eV]	ΔE [eV]
PIDIE-6	^{241}Am	59.54	59.55	60	10
	^{240}Pu	104.23	104.11	62	120
	^{239}Pu	129.3	129.292	64	8
	^{241}Pu	208	207.85	64	146
^{153}Gd	^{153}Gd	97.43	97.447	59	17
PIDIE-1	^{241}Am	59.54	59.56	58	20
	^{240}Pu	104.23	104.3	61	70
	^{239}Pu	129.3	129.31	68	10
	^{241}Pu	208	208.1	74	100
^{166m}Ho/^{57}Co	^{166m}Ho	80.57	80.78	66	210
	^{57}Co	122.06	122.4	65	340
	^{166m}Ho	184.41	184.91	66	500
CBNM61	^{241}Am	59.54	59.54	68	0
	^{240}Pu	104.23	104.08	70	150
	^{239}Pu	129.3	128.83	72	470
	^{241}Pu	208.0	207.84	72	160
A1-324-1	^{235}U	143.76	144	64	240
	^{235}U	185.71	185.97	65	260
			Averages:	65.4	157
			Worst:	74	500

Table 4: Resolution results for eight-hour data set. For each peak given at energy, E, the FWHM is given along with the parameters from a tw-tailed Bortels fit: $2.355 \cdot \sigma$, left tail (τ_L), and right tail fit (τ_R). These four parameters are given for both the average of all the pixels' spectra and the co-added spectrum. The FWHM and fit parameters are all given in eV.

		Average				Co-Added			
Item	E [keV]	FWHM	$2.355 \cdot \sigma$	τ_L	τ_R	FWHM	$2.355 \cdot \sigma$	τ_L	τ_R
PIDIE-6	129.3	57	49	5	6	61	48	13	14
PIDIE-1	129.3	57	51	5	5	58	46	13	13
^{166m}Ho + ^{57}Co	80.6	65	55	7	8	65	51	14	15
CBNM61	129.3	70	60	6	7	71	53	16	17
A1-324-1	143.8	60	54	5	5	64	54	12	12

Table 5: Resolution results for full acquisition data set. For each peak given at energy, E, the FWHM is given along with the parameters from a tw-tailed Bortels fit: $2.355 \cdot \sigma$, left tail (τ_L), and right tail fit (τ_R). These four parameters are given for both the average of all the pixels' spectra and the co-added spectrum. The FWHM and fit parameters are all given in eV.

		Average				Co-Added			
Item	E [keV]	FWHM	$2.355 \cdot \sigma$	τ_L	τ_R	FWHM	$2.355 \cdot \sigma$	τ_L	τ_R
PIDIE-6	129.3	65	57	6	7	64	51	13	13
^{153} Gd	97.4	56	52	4	5	58	49	10	12
PIDIE-1	129.3	65	58	9	6	64	52	13	14
^{166m}Ho + ^{57}Co	80.6	65	55	7	10	64	49	15	16
CBNM61	129.3	76	62	7	11	73	52	18	20
A1-324-1	143.8	64	57	5	8	63	51	12	14

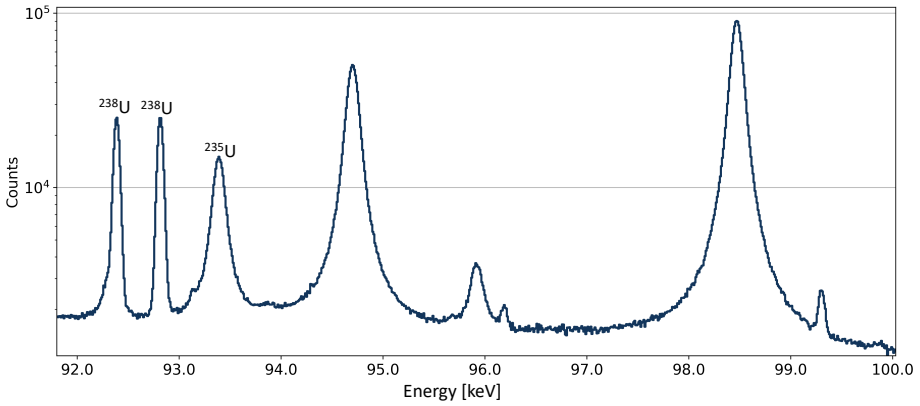

Figure 4: The 90-keV region of co-added 10% enriched uranium A1-324-1 spectrum. Note the clear separation of the ^{238}U signatures at 92.4 and 92.8 keV and the signature at 93.35 keV primarily from ^{235}U that is used for forensics and safeguards.

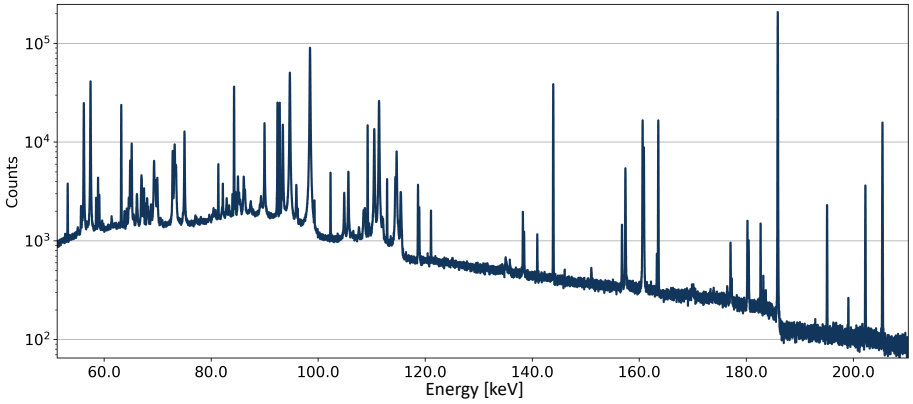

Figure 5: A1-324-1 10% enriched uranium co-added spectrum from 50 to 200 keV.

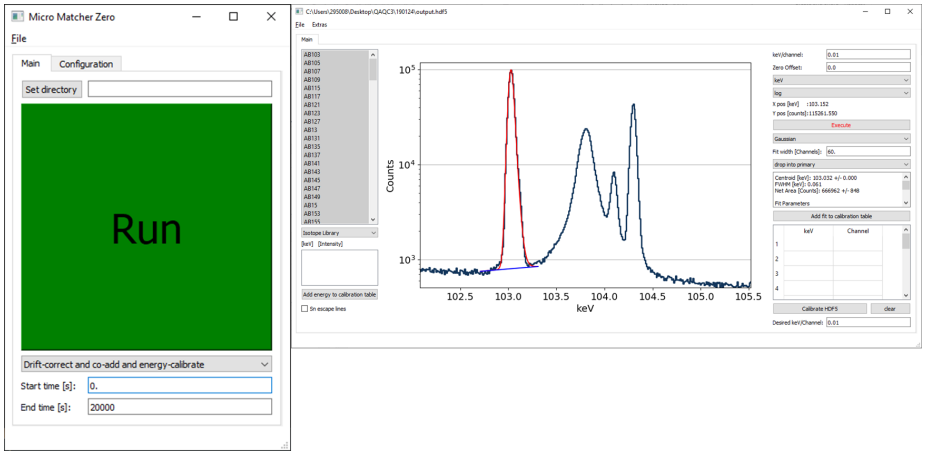

Figure 6: Single-button automated user-interface for co-adding and energy calibration algorithm (left). Visualization, quality assurance, and basic analysis software (right).

information concerning the source being measured. Another advantage of this methodology is the decoupling of the energy calibration from the co-adding. After co-adding and with the benefit of increased statistical precision, any method can be used for the energy calibration of a single spectrum. This work provides an automated algorithm relying on fluoresced tantalum x-rays and tin x-ray escape peaks. Energy calibration is typically within a few hundred eV between 60 and 208 keV for the sources measured in this work.

7. Acknowledgements

This work was supported by the G. T. Seaborg Institute and the US Department of Energy (DOE) Nuclear Energy's Fuel Cycle Research and Development (FCR&D), Materials Protection, Accounting and Control Technologies (MPACT) Campaign.

References

[1] J. A. Mates, D. T. Becker, D. A. Bennett, B. J. Dober, J. D. Gard, J. P. Hays-Wehle, J. W. Fowler, G. C. Hilton, C. D. Reintsema, D. R. Schmidt, D. S. Swetz, L. R. Vale, J. N. Ullom, Simultaneous readout of 128 X-ray and gamma-ray transition-edge microcalorimeters using microwave SQUID multiplexing, Applied Physics Letters 111 (6) (2017). doi:10.1063/1.4986222.

[2] O. Noroozian, J. A. B. Mates, D. A. Bennett, J. A. Brevik, J. W. Fowler, J. Gao, G. C. Hilton, R. D. Horansky, K. D. Irwin, Z. Kang, D. R. Schmidt, L. R. Vale, J. N. Ullom, High-resolution gamma-ray spectroscopy with a microwave-multiplexed transition-edge sensor array, Applied Physics Letters 103 (20) (2013) 202602. doi:10.1063/1.4829156.
URL http://aip.scitation.org/doi/10.1063/1.4829156

[3] D. A. Bennett, J. A. Mates, J. D. Gard, A. S. Hoover, M. W. Rabin, C. D. Reintsema, D. R. Schmidt, L. R. Vale, J. N. Ullom, Integration of

TES microcalorimeters with microwave SQUID multiplexed readout, IEEE Transactions on Applied Superconductivity 25 (3) (jun 2015). doi:10.1109/TASC.2014.2381878.

[4] J. D. Gard, D. T. Becker, D. A. Bennett, J. W. Fowler, G. C. Hilton, J. A. Mates, C. D. Reintsema, D. R. Schmidt, D. S. Swetz, J. N. Ullom, A Scalable Readout for Microwave SQUID Multiplexing of Transition-Edge Sensors, Journal of Low Temperature Physics 193 (3-4) (2018) 485–497. doi:10.1007/s10909-018-2012-2.

[5] R. Winkler, A. S. Hoover, M. W. Rabin, D. A. Bennett, W. B. Doriese, J. W. Fowler, J. Hays-Wehle, R. D. Horansky, C. D. Reintsema, D. R. Schmidt, L. R. Vale, J. N. Ullom, 256-Pixel microcalorimeter array for high-resolution γ-ray spectroscopy of mixed-actinide materials, Nuclear Instruments and Methods in Physics Research, Section A: Accelerators, Spectrometers, Detectors and Associated Equipment 770 (2015) 203–210. doi:10.1016/j.nima.2014.09.049.

[6] S. R. Bandler, E. Figueroa-Feliciano, N. Iyomoto, R. L. Kelley, C. A. Kilbourne, K. D. Murphy, F. S. Porter, T. Saab, J. Sadleir, Non-linear effects in transition edge sensors for X-ray detection, Nuclear Instruments and Methods in Physics Research, Section A: Accelerators, Spectrometers, Detectors and Associated Equipment 559 (2) (2006) 817–819. doi:10.1016/j.nima.2005.12.149.

[7] C. Hollerith, B. Simmnacher, R. Weiland, F. V. Feilitzsch, C. Isaila, J. Jochum, W. Potzel, J. Höhne, K. Phelan, D. Wernicke, T. May, Energy calibration of superconducting transition edge sensors for x-ray detection using pulse analysis, Review of Scientific Instruments 77 (5) (2006) 053105. doi:10.1063/1.2202911.
URL http://aip.scitation.org/doi/10.1063/1.2202911

[8] D. T. Becker, J. A. Mates, G. C. O'Neil, M. W. Rabin, C. D. Reintsema, D. R. Schmidt, D. S. Swetz, P. Szypryt, L. R. Vale, A. L. Wessels, J. N.

Ullom, B. K. Alpert, D. A. Bennett, M. P. Croce, J. W. Fowler, J. D. Gard, A. S. Hoover, Y. I. Joe, K. E. Koehler, Advances in Analysis of Microcalorimeter Gamma-Ray Spectra, IEEE Transactions on Nuclear Science 66 (12) (2019) 2355–2363. doi:10.1109/TNS.2019.2953650.

[9] J. Chen, J. Benesty, Y. Huang, S. Doclo, New insights into the noise reduction Wiener filter, IEEE Transactions on Audio, Speech and Language Processing 14 (4) (2006) 1218–1233. doi:10.1109/TSA.2005.860851.

[10] K. Moody, P. Grant, Nuclear forensic analysis of thorium, Journal of radioanalytical and nuclear chemistry 241 (1) (1999) 157–167.

[11] K. Mayer, M. Wallenius, I. Ray, Nuclear forensics—a methodology providing clues on the origin of illicitly trafficked nuclear materials, Analyst 130 (4) (2005) 433–441.

[12] A. J. Fahey, C. J. Zeissler, D. E. Newbury, J. Davis, R. M. Lindstrom, Postdetonation nuclear debris for attribution, Proceedings of the National Academy of Sciences of the United States of America 107 (47) (2010) 20207–20212. doi:10.1073/pnas.1010631107.

[13] T. L. Burr, T. E. Sampson, D. T. Vo, Statistical evaluation of FRAM γ-ray isotopic analysis data, Applied Radiation and Isotopes 62 (6) (2005) 931–940. doi:10.1016/j.apradiso.2005.01.002.

[14] D. A. Bennett, J. A. Mates, J. D. Gard, A. S. Hoover, M. W. Rabin, C. D. Reintsema, D. R. Schmidt, L. R. Vale, J. N. Ullom, Integration of TES microcalorimeters with microwave SQUID multiplexed readout, IEEE Transactions on Applied Superconductivity 25 (3) (jun 2015). doi:10.1109/TASC.2014.2381878.

[15] M. P. Croce, K. E. Koehler, M. H. Carpenter, M. D. Yoho, S. E. Kossmann, S. E. Garner, M. W. Rabin, D. T. Becker, D. A. Bennett, J. D. Gard, J. A. B. Mates, N. J. Ortiz, D. R. Schmidt, A. L. Wessels, J. Ul-

lom, Practical Microcalorimeter Spectrometers, in: 60th INMM Annual Meeting, Palm Desert, CA, 2019.

[16] G. Bortels, P. Collaers, Analytical function for fitting peaks in alpha-particle spectra from Si detectors, International Journal of Radiation Applications and Instrumentation. Part A. Applied Radiation and Isotopes 38 (10) (1987) 831–837. doi:10.1016/0883-2889(87)90180-8.
URL http://linkinghub.elsevier.com/retrieve/pii/0883288987901808

[17] S. Pommé, B. Caro Marroyo, Improved peak shape fitting in alpha spectra, Applied Radiation and Isotopes 96 (2015) 148–153. doi:10.1016/j.apradiso.2014.11.023.

[18] B. Pritychenko, A. A. Sonzogni, D. F. Winchell, V. V. Zerkin, R. Arcilla, T. W. Burrows, C. L. Dunford, M. W. Herman, V. McLane, P. Obložinskỳ, et al., Nuclear reaction and structure data services of the national nuclear data center, Annals of Nuclear Energy 33 (4) (2006) 390–399.

[19] E. Grushka, I. Atamna, The use of derivatives for establishing integration limits of chromatographic peaks, Chromatographia 24 (1) (1987) 226–232. doi:10.1007/BF02688484.

[20] K. Kitamura, K. Hozumi, Effect of savitzky-golay smoothing on second-derivative spectra, Analytica Chimica Acta 201 (C) (1987) 301–304. doi:10.1016/S0003-2670(00)85349-0.

[21] E. Grushka, D. Israeli, Characterization of Overlapped Chromatographic Peaks by Their Second Derivative. The Limit of the Method, Analytical Chemistry 62 (7) (1990) 717–721. doi:10.1021/ac00206a014.

[22] C. G. Pappas, J. W. Fowler, D. A. Bennett, W. B. Doriese, Y. I. Joe, K. M. Morgan, G. C. O'Neil, J. N. Ullom, D. S. Swetz, A Highly Linear Calibration Metric for TES X-ray Microcalorimeters, Journal of Low

Temperature Physics 193 (3-4) (2018) 249–257. arXiv:1808.00623, doi:10.1007/s10909-018-1999-8.

[23] T. J. Ross, Fuzzy Logic with Engineering Applications, 3rd Edition, John Wiley & Sons, Ltd, 2010.